Simplified stress analysis of multilayered bonded structure under 1D-bar kinematics

Vincent Torrelli, Eric Paroissien *

Institut Clément Ader (ICA), Université de Toulouse, ISAE-SUPAERO, INSA, IMT MINES ALBI, UPS, CNRS, 3 Rue Caroline Aigle, 31400 Toulouse, France

Keywords:
Single-lap bonded joint
Multilayered
Finite element
Macro-element
Taylor expansion power series

A B S T R A C T

Many current materials and structural systems are layered. The structural performances of these multilayered systems are dependent on interfaces, the presence of which is inherent to them. A methodology for the simplified stress analysis of such structures under 1D-bar kinematics is presented. The macro-element technique is used to solve the set of ordinary differential equations involved. A dedicated macro-element is formulated through the approximation of displacements fields by Taylor expansion power series. The predictions of the simplified stress analysis are in close agreements with those obtained by FE analyses. Finally, the influence of adhesive thickness and of the overlap length on the adhesive stress peaks is presented.

1. Introduction

Many current materials and structural systems are layered such as for example, coating systems, electronic packages, multilayered piezoelectric actuators, composite materials, adhesively bonded joints, etc. They are then used in the fields of industrial sectors as varied as automotive, aerospace, energy harvesting or electronics manufacturing. The structural performances of these multilayered systems are dependent on interfaces, the presence of which is inherent to them. The existence of interfaces can be regarded as an opportunity to assign additional functions to the multilayered systems, the integrity of which is dependent on how the load is transferred between the layers. The stress analysis of multilayered systems can be performed thanks to Finite Element (FE) analysis. However, in order to provide accurate predictions, the significant difference between the thickness of layers and interfaces leads to large computational time. It is then beneficial to develop simplified stress analysis for presizing purpose. There have been various studies for stress analysis and sizing for different configurations of bonded joints such as single-lap joint, double-lap, tapered lap joint, etc. However, the studies of multilayered adhesively bonded joints are mainly carried out on the composite laminates adherends. The classical laminate theory is a commonly used predictive tool (evolved in the 1960s) which makes possible the analysis of complex coupling effects that may occur in composite laminates. It is able to predict strains, displacements and curvatures that develop in a laminate when it is loaded [1,2]. On the other hand, the shear-lag method is a tool to analyze the behavior of composite laminates. This method provides for prediction of the mechanical properties of composite interfaces and stress analysis. Nairn defines the transverse variations of shear stress by means of arbitrary shape functions and he derives the shear-lag analysis and solution in term of averages of the new shape functions. These default shape functions can be specified after analysis and adapted for the specific problems [3]. The modifiability property of the shape functions for shear-lag analysis is the strength of this method. Jiang and Peters go further from two-dimensional planar geometries to three-dimensional unidirectional multilayered structures in their study. They derive a shear-lag model for these three-dimensional unidirectional multilayered composite structures. Solution methods are given for several shear stress boundary conditions. They performed the model of an example applied normal stress by means of an equivalent shear stress boundary condition [4]. Viet, Zaki, and Umer introduce a new analytical model to propose for the inter-laminar shear stress in adhesively bonded multilayered metal laminates. In this study, the shear stress function is defined as a mathematical expression of the Young modulus of the adhesive material depending on the metal-to-adhesive thickness ratio in order to know the effect of Young's modulus of the adhesive on the load transfer. The shear-lag mechanism and FE analysis are used to analyze the interfacial behavior of the arbitrary number of laminate layers [5]. This paper provides better understanding of the mechanical behavior of the adhesively bonded laminates and presents an analytical function to be utilized for computation of the inter-laminar shear stress [5].

* Corresponding author.
E-mail address: eric.paroissien@isae-supaero.fr (E. Paroissien).

https://doi.org/10.1016/j.compstruct.2020.112641

Nomenclature

A_j	membrane stiffness of the adherend we_jE_j [mm^2.MPa]
c	half overlap length [mm]
c_1-c_4	integration constant for computation part 2.2.2
C_1, C_2	integration constant for computation part 2.2.1
C	vector gathering c_1-c_4 constants of part 2.2.2
e_j	adherend thickness of layer j [mm]
ea_j	adhesive layer thickness between adherend layers j and j + 1 [mm]
E_j	young modulus of adherend j [MPa]
f_{Lj}	force imposed at left hand of j layer [N]
f_{Rj}	force imposed at right hand of j layer [N]
G_{aj}	shear modulus of adhesive layer between adherends j and j + 1 [MPa]
i	any adherend layers of multilayered bonded joint except layer 1 and P
j	any adherend layers
ka_j	adhesive shear relative stiffness G_j/ea_j [MPa.mm^{-1}]
$[K]$	stiffness matrix of ME
L	overlap length [mm]
Lj	left ME node of layer j
m^{th}	derivative order of displacement
$[M_e]$	matrix of nodal displacements exact solution (ME)
$[M_N]$	matrix of displacement-based approach
n	power series n^{th} term
n_{max}	truncated order of TEPS
N_j	normal force in the adherend j [N]
$[N_e]$	matrix of nodal forces exact solution (ME)
$[N_N]$	matrix of force-based approach
P	last adherend layer of multilayered bonded joint
Q_{Lj}	force imposed at left hand of j layer (ME) [N]
Q_{Rj}	force imposed at right hand of j layer (ME) [N]
$\{Q\}$	vector of applied forces
$\{Q_e\}$	vector of applied forces
Rj	right ME node of layer j
T_j	adhesive shear stress between adherends j and j + 1 [MPa]
u_j	displacement of layer j [mm]
u_{Lj}	displacement of j adherend at left hand of overlap ($x = -c$) [mm]
u_{Rj}	displacement of j adherend at right hand of overlap ($x = c$) [mm]
$U_{j,n}$	coefficient of TEPS method of j adherend
$\{u\}$	vector of displacements
$\{U_e\}$	vector of displacements in ME exact solution
$\{V_N\}$	vector of unknowns
w	overlap width [mm]
x	position along the overlap [mm]
γ_j	adhesive shear angle of any j adhesive layers [rad]
ε_{xx}	normal strain in x-direction
η	constant for computation
λ	constant for computation
ξ	non-dimensional overlap length x/c
σ_{xx}	normal stress in x-direction [MPa]
χ, χ_A	constant for computation
ψ	constant for computation
$[\Psi]$	dummy stiffness matrix

Finally, Pham, Mohareb and Fam develop a FE formulation for the analysis of multilayered beams. The longitudinal normal stress field is defined as Heaviside step function series and polynomial and substituted into the infinitesimal equilibrium conditions to develop expressions for the shear and transverse stress fields. The stress fields thus derived are then adopted within the complementary energy variational principle framework to develop a family of FEs [6]. Sekmen et al. provide a simplified stress analysis of multilayered bonded structure based on the semi-analytical resolution scheme called macro-element (ME) technique [7] under 1D-bar and 1D-beam kinematics. The ME technique is successfully used for the simplified stress analysis of single-lap bonded joints under mechanical and thermal loadings, eventually involving graded materials and geometrical properties along the overlap as well as nonlinear adhesive material behavior, while demanding low computational time [8-11]. Moreover, it is applied to the simulation of the delamination of composite laminated materials under pure mode I for a double cantilever beam test [12]. In this work, the homogeneous properties of composite materials are used for each of both arms, so that the ME used is made of two composite layers linked by one interface layer to be delaminated. The formulation of the stiffness matrix of the multilayered structure by Sekmen et al. is based on the use of exponential matrix. However, even for a linear computation, the results depend on the mesh refinement under 1D-beam kinematics. Besides, a new approach involving the Taylor expansion power series (TEPS) is introduced by Ordonneau et al. [11] to formulate the ME stiffness matrix of two adherends bonded with one adhesive layer. The use of TEPS as a tool in the resolution process has already been employed for simplified stress analysis joints with graded properties [13–16]. The objective of this paper is to present and to assess a methodology for the TEPS-based formulation of the stiffness matrix of the ME of multilayered bonded structures under 1D-bar kinematics. The assessment is performed through the comparison of results coming from a resolution scheme, based on the direct integration of local equilibrium and constitutive equations and from a simplified FE model. The assessment is performed on a unique set of hypotheses: (i) the materials are linear elastic, (ii) only the normal stress is considered in the adherends and (iii) only the in-plane shear stress is considered in the adhesive and is constant through the thickness. This set of hypotheses corresponds to those used by Arnovljevic [17] or Volkersen [18] for the stress analysis of single-lap bonded joints. The good agreement shown validates then the potential application of TEPS-based formulation scheme to the ME of multilayered bonded structures under 1D-beam kinematics.

2. Introduction to simplified stress analysis: Single-Lap bonded joint

2.1. Hypotheses and governing equations

2.1.1. Introduction to shear-lag model

The following hypotheses are taken (i) the adherend layers are linear elastic materials simulated as bars, (ii) the adhesive layer is modelled by an infinite number of linear elastic shear springs linking adherend layers and (iii) the adhesive layer thickness remains constant along the overlap. It results then that (i) only the longitudinal displacements of the neutral line and normal forces are considered in the adherend layers and (ii) all the adhesive stress components vanish except the in-plane shear which is constant in through the thickness. It is then indicated that the shear stress in the adherend layers is not considered in this model. The usual hypothesis of a linear shear stress distribution through the thickness by Tsaï et al. [19] could be easily introduced in the ME formulation following the method provided in [20]. The material and geometrical parameters in the presented models are free; in particular, each adherend layer could have its own Young's modulus.

2.1.2. Single lap bonded joint

The single lap bonded joint (SLJ) shown in the following Fig. 1 is the simplest multilayered bonded joint where two metallic layers are bonded together by a thin layer of adhesive. The Fig. 1 shows a possible configuration for experiment where one layer is clamped and the other is submitted to a tensile load.

Let's define the variable j that identifies the adherend location from the top to bottom $j = 1 \cdots i \cdots P$ where P is the total number of metallic layers and i any layers except the first (1) and the last one (P). In the SLJ, two metallic layers compose the model so that $P = 2$ and $j = 1, 2$. The mechanical and geometrical characteristics of the adherends are respectively given in term module of elasticity E_j and thickness e_j. Also, it has to be reminded that all the layers (adherends/adhesives) will have the same width w all along this paper. From the 1D-bar definition, the normal force in the adherend at any location$j$ can be written by the equation Eq. (1).

$$N_j = A_j \frac{du_j}{dx} \tag{1}$$

with A_j being the membrane stiffness of the adherends:

$$A_j = we_jE_j \tag{2}$$

There is a relative displacement between the top and the bottom boundary of the adhesive layer:

$$\Delta u_j(x) = u_{j+1} - u_j \tag{3}$$

This relative displacement induces a shear stress in the adhesive layer characterized by the shear angle γ as shown in the Fig. 2:

It is assumed that small displacements are considered so that the shear angle γ_j and the corresponding shear stress T_j are written below. Note that the adhesive shear modulus is G_j.

$$\gamma_j \approx \tan(\gamma_j) = \frac{\Delta u_j}{ea_j} = \frac{u_{j+1} - u_j}{ea_j} \tag{4}$$

$$T_j = G_{aj}\gamma_j = \frac{G_{aj}}{ea_j}(u_{j+1} - u_j) \tag{5}$$

The shear stress in any j adhesive layers is thus:

$$T_j = ka_j(u_{j+1} - u_j) \tag{6}$$

with

$$ka_j = \frac{G_{aj}}{ea_j} \tag{7}$$

In any size of multilayered bonded joint, the adhesive layers will always be surrounded by two adherends so that the number of adhesive layers will be equal to $(P-1)$. Consequently, the location of adhesive layers will be $j = 1 \cdots i \cdots (P-1)$. In the case of SLJ, $j = 1$:

$$T_1 = ka_1(u_2 - u_1) \tag{8}$$

Since the constitutive equations of all substrates are known, the study of the local equilibrium in each of the adherends is performed. As shown in Fig. 3, an elementary part of length $dx$of the overlap is considered and a static analysis along the x-axis is performed.Fig 4.

The general expressions of the normal force as a function of the adhesive shear stress obtained is:

$$\frac{dN_j}{dx} = (-1)^j wT_j \tag{9}$$

2.2. Exact solution

In order to verify the future results, an exact solution of the SLJ model must first be obtained.

2.2.1. Exact closed-form solution

In this part, the exact solution of the normal forces and adhesive shear stress of the SLJ is presented. The solution by algebraic manipulation and simple differential equation solving.

$$N_2 = C_1e^{-\eta x} + C_2e^{\eta x} - \lambda f \tag{10}$$

with the constants:

$$\eta^2 = \frac{G_{a1}}{ea_1}\left(\frac{1}{E_2e_2} - \frac{1}{E_1e_1}\right) \tag{11}$$

$$\lambda = -\frac{1}{1 + \frac{E_1e_1}{E_2e_2}} \tag{12}$$

$$C_1 = \left(\frac{\lambda(e^{\eta L} - 1) - 1}{2\sinh(\eta L)}\right)f \tag{13}$$

$$C_2 = \left(\frac{\lambda(1 - e^{-\eta L}) + 1}{2\sinh(\eta L)}\right)f \tag{14}$$

To obtain the shear stress of the adhesive along the overlap, equation Eq. (10) is integrated along x such that:

$$T_1 = \frac{1}{w}\frac{dN_2}{dx} \tag{15}$$

2.2.2. Exact ME stiffness matrix

In this part, a SLJ will be reduced into a ME. The ME technique is the methodology for the simplified stress analysis of bonded joints. Based on simplified hypotheses, the actual joint is meshed in particular elements. The bonded overlap are modeled by dedicated 4-nodes Bonded-bars (BBa). Only one BBa, depending on the chosen kinematics, is sufficient to be representative for an entire bonded overlap in the frame of a linear elastic analysis. The ME technique is inspired by the FE method and differs in the sense that the interpolation functions are not assumed. Indeed, they take the shape of solutions of the

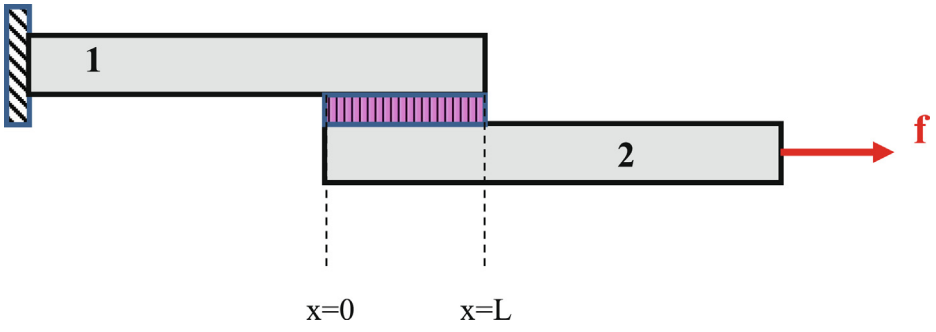

Fig. 1. Representation of single lap bonded joints in tensile test configuration.

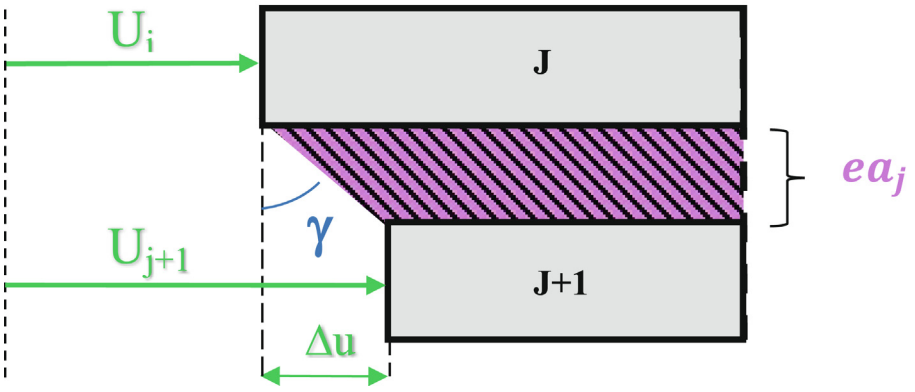

Fig. 2. Adherends relative displacement and shear angle presentation.

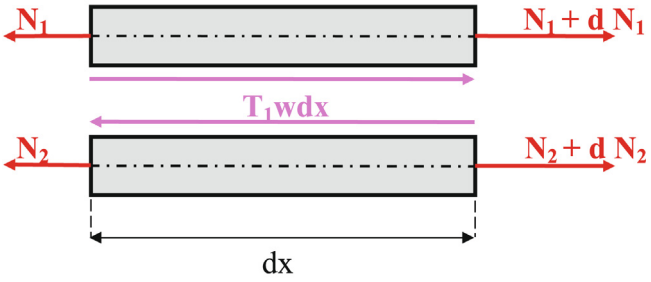

Fig. 3. Representation of adherend local equilibrium.

governing ordinary differential equations (ODEs) system, coming from the constitutive equations of the adhesives and adherends and from the local equilibrium equations, related to the simplifying hypotheses. The main work is thus the formulation of the elementary stiffness matrix of the ME. Once the stiffness matrix of the complete structure is assembled from the elementary matrices and the boundary conditions are applied, the minimization of the potential energy provides the solution, in terms of adhesive stress distributions along the overlap, internal forces and displacements in the adherends. The ME technique can be regarded as mathematical procedure allowing for the resolution of the system of ODE, under a less restricted application field of simplifying hypotheses, in terms of geometry, material behaviors, kinematics, boundary conditions and loads.

As shown in the figure below, the SLJ will be transformed into a ME which is no more than a system of four nodes linked by a 4×4 stiffness matrix K:

Note that for the four nodes $L1, L2, R1, R2$, the letter means the "Left" or the "Right" of the bar and the number stands for the number of the bar. Also, for a measure of convenience (used later), the overlap length now goes from $-c$ to c where c represents the half length of then overlap. In order to find the exact stiffness matrix K_e of the SLJ, the constitutive equations have been gathered in a system. Starting by local equilibrium equations, the adhesive shear stress has been injected. Then, equations of normal forces have been differentiated according to x and injected to the set of equations. The system obtained is presented below in Eq. (16).

$$\begin{cases} \frac{d^2u_1}{dx^2} + \frac{wka_1}{A_1}(u_2 - u_1) = 0 \\ \frac{d^2u_2}{dx^2} - \frac{wka_1}{A_2}(u_2 - u_1) = 0 \end{cases} \tag{16}$$

The system is a set of coupled differential equations where the general solution for the unknowns (the displacements) are presented below in Eqs. (17) and (18):

$$u_1(x) = \frac{1}{2}(c_1 + c_2 x - c_3(1+\chi)e^{-\eta x} - c_4(1+\chi)e^{\eta x}) \tag{17}$$

$$u_2(x) = \frac{1}{2}(c_1 + c_2 x - c_3(1+\chi)e^{-\eta x} - c_4(1+\chi)e^{\eta x}) \tag{18}$$

with:

$$\chi = \frac{\psi^2}{\eta^2} \tag{19}$$

$$\psi^2 = \frac{G_{a1}}{ea_1}\left(\frac{1}{e_1E_1} - \frac{1}{e_2E_2}\right) \tag{20}$$

$$\eta^2 = \frac{G_{a1}}{ea_1}\left(\frac{1}{e_1E_1} + \frac{1}{e_2E_2}\right) \tag{21}$$

And c_1,c_2, c_3 and c_4 are integration constants. The boundary conditions at both extremities of the ME, in terms of displacements, lead to the expressions for the integration constants as a function of nodal displacements u_{L1},u_{L2}, u_{R1},u_{R2}. These integration constants are gathered in a vector:

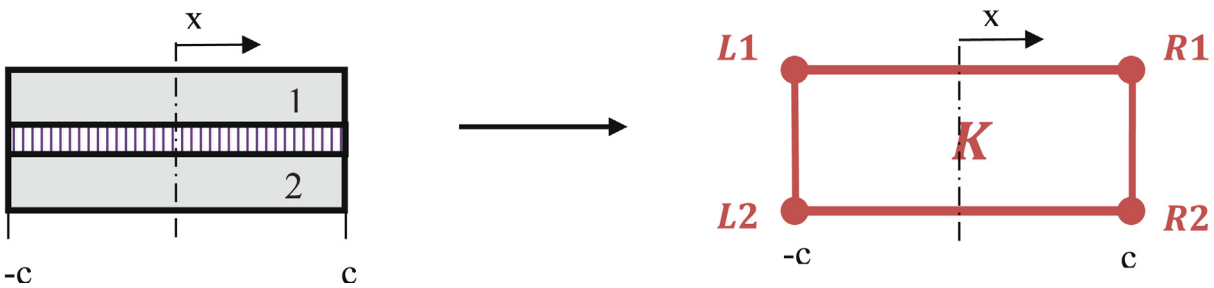

Fig. 4. Physical single lap model transformed into ME.

$$C = \begin{pmatrix} c_1 \\ c_2 \\ c_3 \\ c_4 \end{pmatrix} = {M_e}^{-1} U_e \tag{22}$$

with:

$${M_e}^{-1} = \begin{pmatrix} (1-\chi) & (1+\chi) & 0 & 0 \\ -\frac{(1-\chi)}{2c} & -\frac{(1+\chi)}{2c} & \frac{(1-\chi)}{2c} & \frac{(1+\chi)}{2c} \\ -\frac{e^{2\eta c}}{2\sinh(2\eta c)} & \frac{e^{2\eta c}}{2\sinh(2\eta c)} & \frac{1}{2\sinh(2\eta c)} & -\frac{1}{2\sinh(2\eta c)} \\ \frac{e^{-2\eta c}}{2\sinh(2\eta c)} & -\frac{e^{-2\eta c}}{2\sinh(2\eta c)} & -\frac{1}{2\sinh(2\eta c)} & \frac{1}{2\sinh(2\eta c)} \end{pmatrix} \tag{23}$$

The nodal forces are then computed from the constitutive equations:

$$N_1(x) = \frac{1}{2}(c_2 + c_3\eta(1+\chi)e^{-\eta x} - \eta c_4(1+\chi)e^{\eta x})A_1 \tag{24}$$

$$N_2(x) = \frac{1}{2}(c_2 - c_3\eta(1-\chi)e^{-\eta x} + \eta c_4(1-\chi)e^{\eta x})A_2 \tag{25}$$

The nodal normal forces are then deduced as function of the integration constants:

$Q_e = N_e {M_e}^{-1} U_e$(26)with:

$$N_e = \frac{1}{2}\begin{pmatrix} 0 & -A_1 & -\eta(1+\chi)A_1 & \eta(1+\chi)A_1 \\ 0 & -A_2 & \eta(1-\chi)A_2 & -\eta(1-\chi)A_2 \\ 0 & A_1 & \eta(1+\chi)e^{-2\eta c}A_1 & -\eta(1+\chi)e^{2\eta c}A_1 \\ 0 & A_2 & -\eta(1-\chi)e^{-2\eta c}A_2 & \eta(1-\chi)e^{2\eta c}A_2 \end{pmatrix} \tag{27}$$

Then it comes:

$$Q_e = N_e {M_e}^{-1} U_e \tag{28}$$

The elementary stiffness matrix is finally computed from the matrix M_e and N_e:

$$K_e = N_e {M_e}^{-1} = \frac{1}{1+\chi_A}\frac{A_2}{2c} \begin{pmatrix} \frac{2\eta c}{\tanh(2\eta c)} + \frac{1}{\chi_A} & 1 - \frac{2\eta c}{\tanh(2\eta c)} & -\frac{2\eta c}{\sinh(2\eta c)} - \frac{1}{\chi_A} & \frac{2\eta c}{\sinh(2\eta c)} - 1 \\ 1 - \frac{2\eta c}{\tanh(2\eta c)} & \frac{2\eta c}{\tanh(2\eta c)} + \chi_A & \frac{2\eta c}{\sinh(2\eta c)} - 1 & -\frac{2\eta c}{\sinh(2\eta c)} - \chi_A \\ -\frac{2\eta c}{\sinh(2\eta c)} - \frac{1}{\chi_A} & \frac{2\eta c}{\sinh(2\eta c)} - 1 & \frac{2\eta c}{\tanh(2\eta c)} + \frac{1}{\chi_A} & 1 - \frac{2\eta c}{\tanh(2\eta c)} \\ \frac{2\eta c}{\sinh(2\eta c)} - 1 & -\frac{2\eta c}{\sinh(2\eta c)} - \chi_A & 1 - \frac{2\eta c}{\tanh(2\eta c)} & \frac{2\eta c}{\tanh(2\eta c)} + \chi_A \end{pmatrix} \tag{29}$$

with:

$$\chi_A = \frac{A_2}{A_1} \tag{30}$$

The 4×4 exact stiffness matrix $K_e$of the SLJ ME using Volkersen assumption is thus obtained in Eq. (29):

2.3. TEPS solution

In the part, the Taylor Expansion into Power Series (TEPS) resolution scheme will be introduced. This method will be used to decouple and linearize a complex system of differential equations. The main assumption is that the displacements (unknowns) are written under the following form:

$$u_j(x) = \sum_{n=0}^{\infty} \mathrm{u}_{j,n} x^n = \sum_{n=0}^{\infty} \mathrm{U}_{j,n} \xi^n \tag{31}$$

with:

$$\xi = \frac{x}{c} \tag{32}$$

For the series terms to have the same unit as the function approximated, the variable change of Eq. (32) is introduced. As a result, the solution is searched for anyξincluded between -1 and 1. The advantages of this non-dimensionalization is that the polynomial will now vary from -1 to 1 which avoids dealing with big numbers elevated at high power. On the other hand, the any m^{th} derivative equation of $u_j(x)$ must be introduced:

$$\frac{d^m u_j}{dx^m} = \frac{1}{c^m}\frac{d^m u_j}{d\xi^m} = \frac{1}{c^m}\sum_{n=0}^{\infty}\prod_{i=1}^{m}(n+i)U_{n+m}\xi^n \tag{33}$$

2.3.1. TEPS analytical solution

In this part, the SLJ model will be developed using the TEPS equations presented in the previous part. The non-linear system of coupled differential equations presented in Eq. (16) is rewritten using the TEPS fundamental equations Eqs. (31)–(33):

$$\begin{cases} \mathrm{U}_{1,n+2} + \frac{wc^2}{A_1(n+1)(n+2)} ka_1(\mathrm{U}_{2,n} - \mathrm{U}_{1,n}) = 0 \\ \mathrm{U}_{2,n+2} - \frac{wc^2}{A_2(n+1)(n+2)} ka_1(\mathrm{U}_{2,n} - \mathrm{U}_{1,n}) = 0 \end{cases} \tag{34}$$

Thanks to the TEPS assumption, the system Eq. (16) became system Eq. (34) which is a linear system of coupled differential equations called “recursive equations” and easily solvable.

This system is then truncated at an n_{max} order and is $2(n_{max}-1)$ big. To this set of recursive equations, two boundary equations per adherend must be added to retrieve a balanced system. As shown is Fig. 5 below, the boundary conditions can either be forces or displacements.

Using TEPS assumption Eq. (31), the boundary conditions in displacement can be written:

$at\xi = -1 : \sum_{n=0}^{\infty} \mathrm{U}_{j,n}(-1)^n = \mathrm{u}_{Lj}$(35)

$$at\xi = 1 : \sum_{n=0}^{\infty} \mathrm{U}_{j,n} = \mathrm{u}_{Rj} \tag{36}$$

Using fundamental equation Eq. (5) and TEPS assumption the boundary conditions in force can be written:

$$at\xi = -1 : \frac{A_j}{c}\sum_{n=0}^{\infty}(-1)^n(\mathrm{n}+1)\mathrm{U}_{j,n+1} = Q_{Lj} \tag{37}$$

$$at\xi = 1 : \frac{A_j}{c}\sum_{n=0}^{\infty}(\mathrm{n}+1)\mathrm{U}_{j,n+1} = Q_{Rj} \tag{38}$$

Finally, by gathering system Eq. (34) of the size $2(n_{max}-1)$ with any set of four boundary condition equations from Eqs. (35)–(38), the obtained system is balanced and is of the size $2(n_{max}+1)$. The system can easily be solved by putting it into matrix form and solving it like any linear systems where the vector of unknowns V_N is the TEPS coefficients $\mathrm{U}_{j,n}$ collection:

$$\{V_N\} = [\mathrm{U}_{1,0}\mathrm{U}_{1,1}\cdots\mathrm{U}_{1,nmax}\mathrm{U}_{2,0}\cdots\mathrm{U}_{2,nmax}]^T \tag{39}$$

2.3.2. TEPS ME stiffness matrix

As in the part *2.2.2*, the starting equation is the system Eq. (16). From this system, two different systems will be derived, one using displacements as unknown and the other using normal forces as unknown. At the end, few manipulations will lead to the presentation of the ME stiffness matrix using TEPS assumption.

In this part, the system Eq. (16) will be written into matrix form focusing on the displacements. The displacements $u_{L1}, u_{L2}, u_{R1}, u_{R2}$ of the four nodes of ME introduced in Fig. 6 are the unknowns to determine.

As derived in part 2.3.1, by considering the displacements as unknowns, the system Eq. (16) became Eq. (34). Then, four boundary conditions in term of displacements must be found so that the system is balanced. The equations used are Eq. (35) and Eq. (36) which gives:

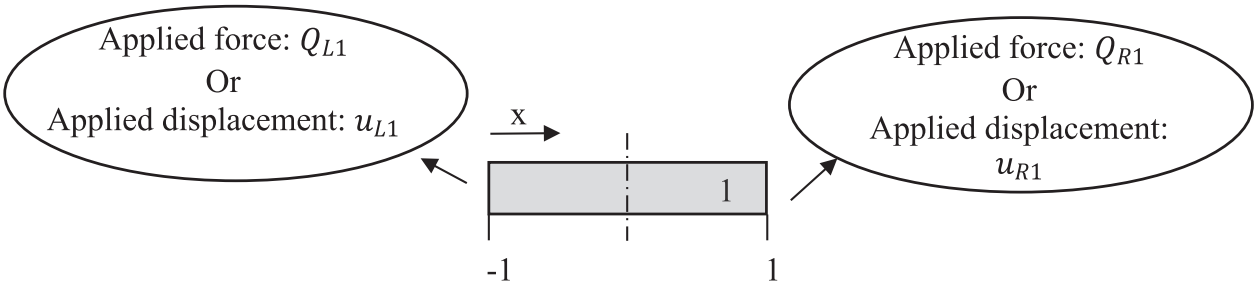

Fig. 5. Application of boundary condition at overlap ends.

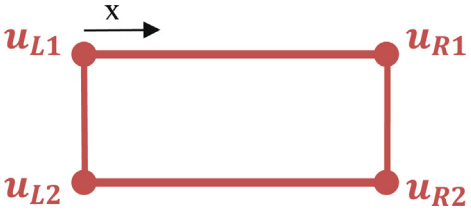

Fig. 6. Applied displacement on SLJ ME.

$$at\xi = -1 : \begin{cases} \sum_{n=0}^{\infty} U_{1,n}(-1)^n = u_{L1} \\ \sum_{n=0}^{\infty} U_{2,n}(-1)^n = u_{L2} \end{cases} \tag{40}$$

$$at\xi = -1 : \begin{cases} \sum_{n=0}^{\infty} U_{1,n} = u_{R1} \\ \sum_{n=0}^{\infty} U_{2,n} = u_{R2} \end{cases} \tag{41}$$

Finally, the three above systems Eq. (34), Eqs. (40)–(41) are assembled which give a balanced system of the size $2(n_{max}+1)$. The system can now be put into matrix form.

The vector V_N introduced before is still the unknown coefficients vector. Then, the dummy displacements vector $u$that gathers the right hand of the equations is introduced:

$$\{u\} = \left[0 \times 2(n_{max}-1) u_{L1} u_{L2} u_{R1} u_{R2}\right]^T \tag{42}$$

Note that V_N and u are of the size $2(n_{max}+1)\times 1$. Finally, the matrix form of the complete system is thus:

$$[M_N]\{V_N\} = \{u\} \tag{43}$$

with the matrix M_N of the size $[2(n_{max}+1)]^2$.

In this part, the system Eq. (16) will be written into matrix form focusing on the forces. As shown in the Fig. 7, the normal forces $Q_{L1}, Q_{L2}, Q_{R1}, Q_{R2}$ applied on the four nodes of the ME are the unknowns to determine.

In the force based approach, manipulation is required to write the system Eq. (16) with normal forces only. First, the system Eq. (16) has been differentiated with respect to x such that:

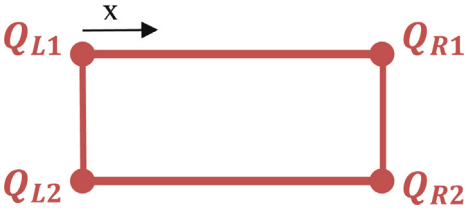

Fig. 7. Applied displacement on SLJ ME.

$$\begin{cases} \frac{d^3u_1}{dx^3} + \frac{wka_1}{A_1}\left(\frac{du_2}{dx} - \frac{du_1}{dx}\right) = 0 \\ \frac{d^3u_2}{dx^3} - \frac{wka_1}{A_2}\left(\frac{du_2}{dx} - \frac{du_1}{dx}\right) = 0 \end{cases} \tag{44}$$

Then, using Eq. (5) and its derivatives, the system Eq. (44) became:

$$\begin{cases} \frac{d^2N_1}{dx^2} + wka_1\left(\frac{N_2}{A_2} - \frac{N_1}{A_1}\right) = 0 \\ \frac{d^2N_2}{dx^2} - wka_1\left(\frac{N_2}{A_2} - \frac{N_1}{A_1}\right) = 0 \end{cases} \tag{45}$$

Thus, the normal force and its derivative became:

$$N_j = A_j\frac{du_j}{dx} = \frac{A_j}{c}\sum_{n=0}^{\infty}(n+1)U_{j,n+1}\xi^n \tag{46}$$

$$\frac{d^2N_j}{dx^2} = A_j\frac{d^3u_j}{dx^3} = \frac{A_j}{c^3}\sum_{n=0}^{\infty}(n+1)(n+2)(n+3)U_{j,n+3}\xi^n \tag{47}$$

Finally, the system of coupled differential equations in TEPS form (force approach) is:

$$\begin{cases} U_{1,n+3} + \frac{wc^2}{A_1(n+2)(n+3)}ka_1(U_{2,n+1} - U_{1,n+1}) = 0 \\ U_{2,n+3} - \frac{wc^2}{A_2(n+2)(n+3)}ka_1(U_{2,n+1} - U_{1,n+1}) = 0 \end{cases} \tag{48}$$

This system is then truncated at an *nmax* order and is $2(n_{max}-2)$ big. To this set of recursive equations, two boundary equations per adherend must be added to retrieve a balanced system. First, using the equations of the TEPS part, the boundary equations at the left part ($\xi = -1$) are:

$$\begin{cases} -\frac{A_1}{c}\sum_{n=0}^{\infty}(-1)^n(n+1)U_{1,n+1} = Q_{L1} \\ -\frac{A_2}{c}\sum_{n=0}^{\infty}(-1)^n(n+1)U_{2,n+1} = Q_{L2} \end{cases} \tag{49}$$

Second, using the equations of the TEPS part, the boundary equations at the right part ($\xi = 1$) are:

$$\begin{cases} \frac{A_1}{c}\sum_{n=0}^{\infty}(n+1)U_{1,n+1} = Q_{R1} \\ \frac{A_2}{c}\sum_{n=0}^{\infty}(n+1)U_{2,n+1} = Q_{R2} \end{cases} \tag{50}$$

Finally, the three above systems Eqs. (48)–(50) are assembled which gives a system of the size $2n_{max}$. Two lines of zeros are added in order to balance the system so that its size became$2(n_{max}+1)$. The system can now be put into matrix form. The vector V_N remains unchanged but the vector Q is defined as followed:

$$\{Q\} = \left[(0 \times 2(n_{max}-2) + 0 \times 2)Q_{L1}Q_{L2}Q_{R1}Q_{R2}\right]^T \tag{51}$$

The complete system is thus written as followed:

$$[N_N]\{V_N\} = \{Q\} \tag{52}$$

with the matrix N_N of the size $[2(n_{max}+1)]^2$.

Up to now, two linear systems have been obtained. The one of the displacement approach and the one of the force approach. Both systems are of the size $2(n_{max}+1)$ and thus, are compatible for any algebraic manipulation. The aim is to get the stiffness matrix such that:

$$[K]\{u\} = \{Q\} \tag{53}$$

From displacement approach the vector V_N is rewritten as followed:

$$\{V_N\} = [M_N]^{-1}\{u\} \tag{54}$$

Injecting Eq. (54) into force approach Eq. (52) gives:

$$[N_N][M_N]^{-1}\{u\} = [\Psi]\{u\} = \{Q\} \tag{55}$$

Even though u contains values of displacements, it is not really a displacement vector. Similarly for Q. Consequently, the matrix Ψ of the size $[2(n_{max}+1)]^2$ is not the true stiffness matrix of the ME. To do so, the obtained system is reduced by removing the lines and columns of zeros. The vectors u and $Q$are now respectively the true displacements and forces vectors.

$$\{u\} = [u_{L1}u_{L2}u_{R1}u_{R2}]^T \tag{56}$$

$$\{Q\} = [Q_{L1}Q_{L2}Q_{R1}Q_{R2}]^T \tag{57}$$

The stiffness matrix K of the macro-element is a four-by-four square matrix extracted fromΨ:

$$\Psi = [N_N][M_N]^{-1} = \begin{bmatrix} & & 2(nmax-1) \\ & K & \\ & & 2(nmax+1) \end{bmatrix} \tag{58}$$

The stiffness matrix of the ME for the SLJ model is thus:

$$K = [N_N][M_N]^{-1}\begin{matrix} 2(n_{max}-1)\cdots 2(n_{max}+1) \\ 2(n_{max}-1)\cdots 2(n_{max}+1) \end{matrix} \tag{59}$$

2.4. Convergence and comparison

In this part, the results obtained will be compared to the exact solutions to determine the validity and level of accuracy of the TEPS solution scheme.

2.4.1. TEPS scheme

In order to perform the validation, a numerical test specimen similar to the one presented in Fig. 1 has been used. The top adherend (#1) is clamped while the bottom one (#2) is submitted to a tensile load of 100N. Both adherends are made of aluminium and the mechanical and physical properties are presented in the Table 1 below. The data observed during this experiment will be the normal forces in both adherends and the adhesive shear stress.

Table 1
Physical and mechanical properties of SLJ test model.

e_1, e_2	2.5mm
ea_1	0.1mm
c	23mm
w	1mm
E_1 , E_2	72400MPa
G_1	357MPa
f	100N

As discussed previously, the series are truncated at an order n_{max}. However, before comparing anything, the truncated order must be determined so that convergence is obtained. To do so, the normal force in the bottom adherend has been plotted while varying the truncating order as shown in Fig. 8 below.

As pointed out by the arrow, the convergence is fast and occurs around $n_{max} = 15$. The value 15 as been picked so that the maximum error compared to the exact solution is equal to 0.63%. For the following results, this convergence truncated order will be kept. Note that increasing $nmax$ will reduce the percentage error (e.g.: at $n_{max} = 20$, $error = 1,45e^{-4}\%$)

Since convergence order has been identified, results can now be presented. The normal forces in both adherends obtained from exact solution and TEPS solution is compared in Fig. 9 below:

The curves are perfectly superposed and the maximum error between exact and TEPS solution is equal to 0.63%. Similarly, the adhesive shear stress obtained from exact solution has been compared to the TEPS solution. Results are presented below in Fig. 10.

Once again, both curves fit perfectly so that the maximum error between both solutions is equal to 0.087%. Consequently, the TEPS is a very accurate method to approach the exact solution of the mechanical behavior of a SLJ.

3. Simplified stress analysis of multilayered metallic bonded joint

In part *2*, a simplified stress analysis methodology has been introduced in order to predict behaviour of single lap bonded joints. In this part, the same methodology will be applied to any size of multilayered bonded joints.

3.1. Hypotheses and governing equation

The 1D-bar assumptions presented in part 2.1.1 will remain the same. Indeed, the normal forces in any adherend is defined by Eq. (1) and the adhesive layer shear stress is given by Eq. (8). The multilayered model is composed of P-layers of adherends and P-1-layers of adhesives. As shown in the Fig. 11 below, the model is divided into three parts: the first one corresponds to the first adherend ($j = 1$), the second at the adherend i and the third at the last layer called P-layer. Note that as introduced before, j identifies the adherend location: $j = 1 \cdots i \cdots P$.

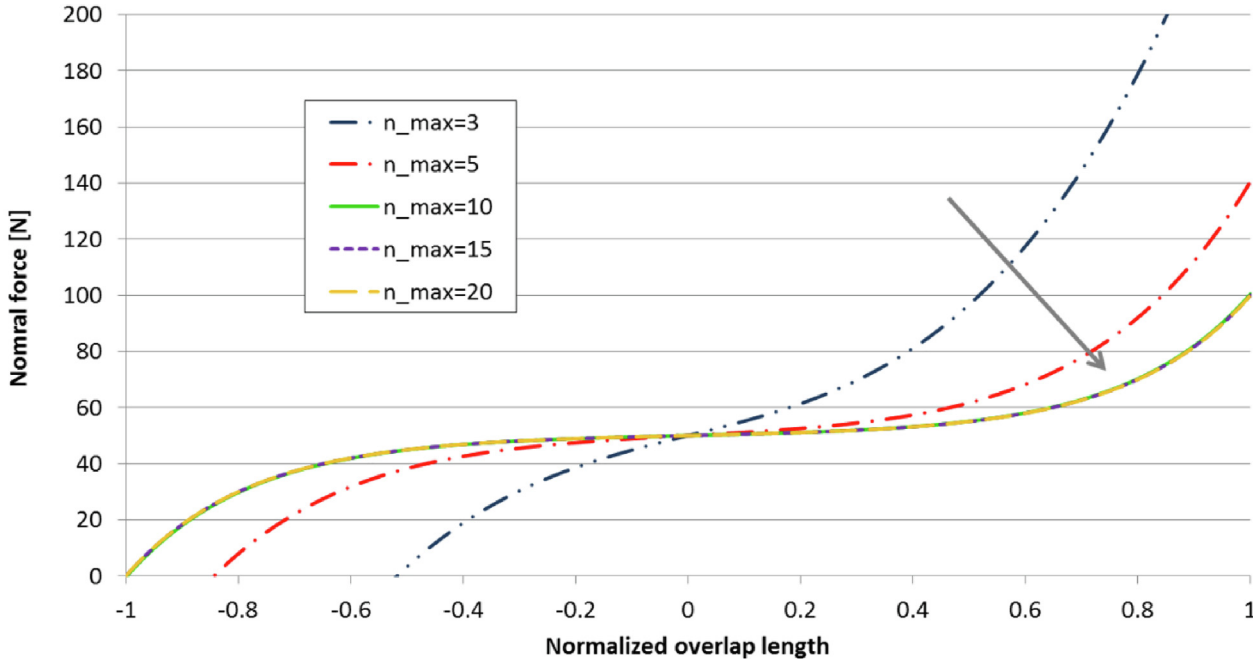

Fig. 8. Convergence of adherend normal force increasing n_{max}.

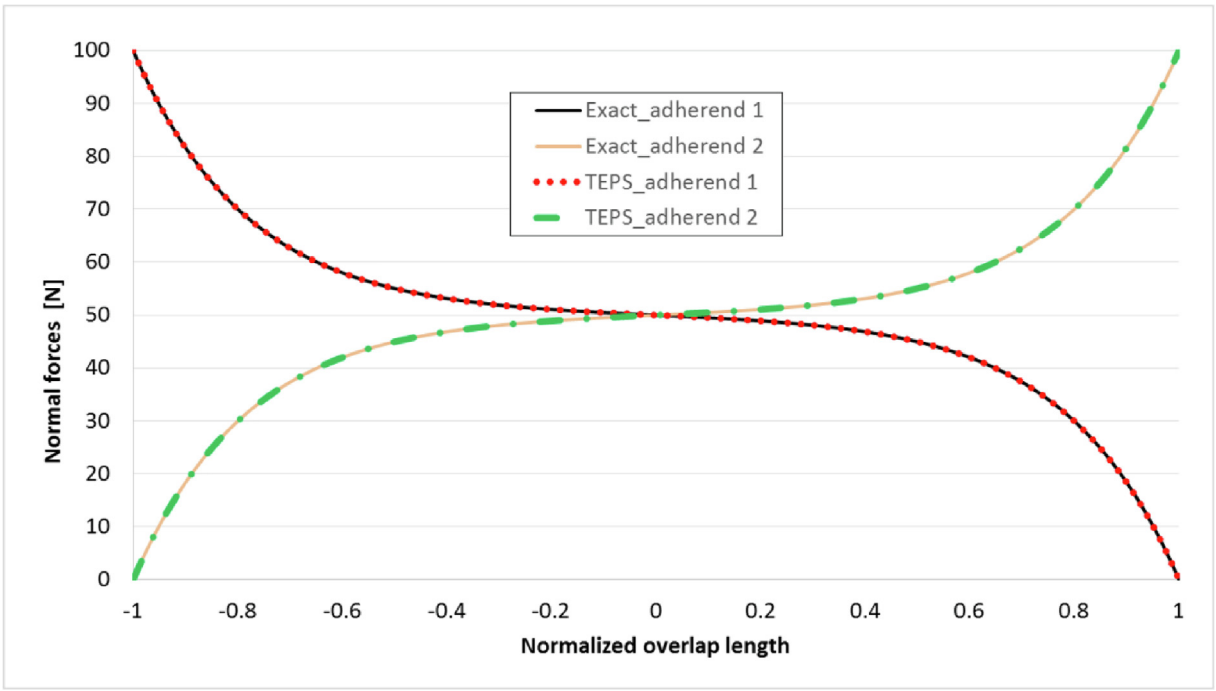

Fig. 9. Exact VS. TEPS solution of normal forces in adherends.

As in the previous part, the local equilibrium is done as shown in Fig. 12.

Then, the equations are gathered under a system of local equilibrium equations.

$$\begin{cases} \frac{dN_1}{dx} + wT_1 = 0 \\ \vdots \\ \frac{dN_i}{dx} + w(T_i - T_{i-1}) = 0 \\ \vdots \\ \frac{dN_P}{dx} - wT_{P-1} = 0 \end{cases} \quad (60)$$

The system Eq. (60) is the raw system of coupled differential equations to be solved.

3.2. TEPS solution

As in the single lap bonded joint part, the unknowns chosen to build the system are the adherends displacements $u_1 \ldots u_i \ldots u_p$.

$$u_j(x) = \sum_{n=0}^{\infty} \mathrm{U}_{j,n}\xi^n with \mathrm{U}_{j,n} = c^n u_{j,n} \quad (61)$$

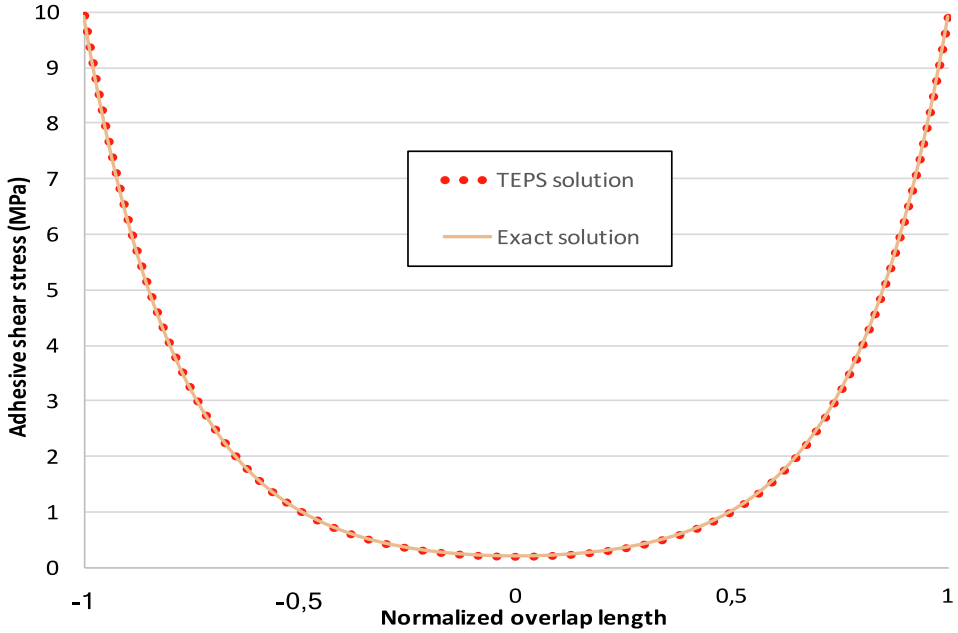

Fig. 10. Exact VS. TEPS solution of adhesive shear stress.

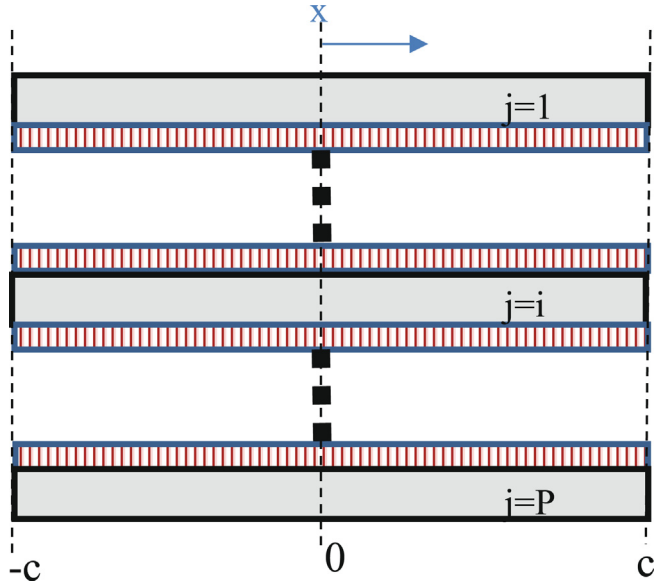

Fig. 11. Multilayered bonded joint configuration.

3.2.1. TEPS analytical solution

Differentiating equation Eq. (1) according to x gives:

$$\frac{d^2u_j}{dx} = \frac{1}{A_j}\frac{dN_j}{dx} \tag{62}$$

Using Eq. (1) and Eq. (6) the system Eq. (60) becomes:

$$\begin{cases} \frac{d^2u_1}{dx} = -\frac{w}{A_1}ka_1(u_2 - u_1) \\ \vdots \\ \frac{d^2u_i}{dx} = \frac{w}{A_i}\left[-u_{i-1}ka_{i-1} + u_i(ka_{i-1} + ka_i) - u_{i+1}ka_i\right] \\ \vdots \\ \frac{d^2u_p}{dx} = \frac{w}{A_p}ka_{p-1}(u_p - u_{p-1}) \end{cases} \tag{63}$$

Using TEPS assumptions shown in Eq. (61) the system Eq. (63) becomes:

$$\begin{cases} \mathrm{U}_{1,n+2} + \frac{wc^2}{A_1(n+1)(n+2)}ka_1(\mathrm{U}_{2,n} - \mathrm{U}_{1,n}) = 0 \\ \vdots \\ \mathrm{U}_{i,n+2} + \frac{wc^2}{A_i(n+1)(n+2)}\left[ka_{i-1}\mathrm{U}_{i-1,n} - (ka_{i-1} + ka_i)\mathrm{U}_{i,n} + ka_i\mathrm{U}_{i+1,n}\right] = 0 \\ \vdots \\ \mathrm{U}_{p,n+2} + \frac{wc^2}{A_p(n+1)(n+2)}ka_{p-1}(\mathrm{U}_{p-1,n} - \mathrm{U}_{p,n}) = 0 \end{cases} \tag{64}$$

Finally, the series are truncated at an order *nmax* so that the number of recursive equations obtained is $P(n_{max} - 1)$. Now, as previously, two boundary conditions per adherend (either in displacement or in force) must be added to system of recursive equations Eq. (64) to balance it. Consequently, $2 \times P$ boundaries are required so that the final size of the system is $P(n_{max} + 1)$. Thus, since the system of equations is now balanced, it is possible to solve the same way as described in part *2.3.1.*

3.2.2. TEPS ME stiffness matrix

In this part, following the previous methodology, the multilayered bonded joint model will be reduced into a ME.

In this part, the previous system Eq. (60) will be written into matrix form focusing on the displacements. The displacements $u_{L1} \cdots u_{Lp}$ and $u_{R1} \cdots u_{Rp}$ of the $2 \times P$ nodes of the ME (shown in Fig. 13) are the unknowns to determine. The system of recursive equations is the one presented in Eq. (64). The set of $2 \times P$ displacement boundary condition equations:

$$\text{At } \xi = -1 : \begin{cases} \sum_{n=0}^{\infty}\mathrm{U}_{1,n}(-1)^n = u_{L1} \\ \vdots \\ \sum_{n=0}^{\infty}\mathrm{U}_{i,n}(-1)^n = u_{Li} \\ \vdots \\ \sum_{n=0}^{\infty}\mathrm{U}_{p,n}(-1)^n = u_{Lp} \end{cases} \tag{65}$$

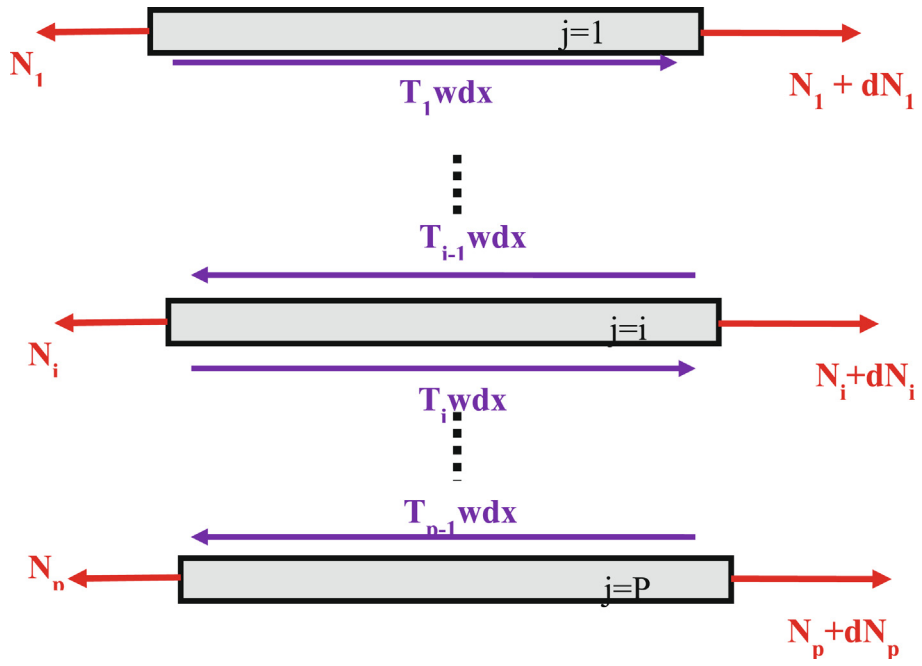

Fig. 12. Local equilibrium representation of multilayered bonded joint.

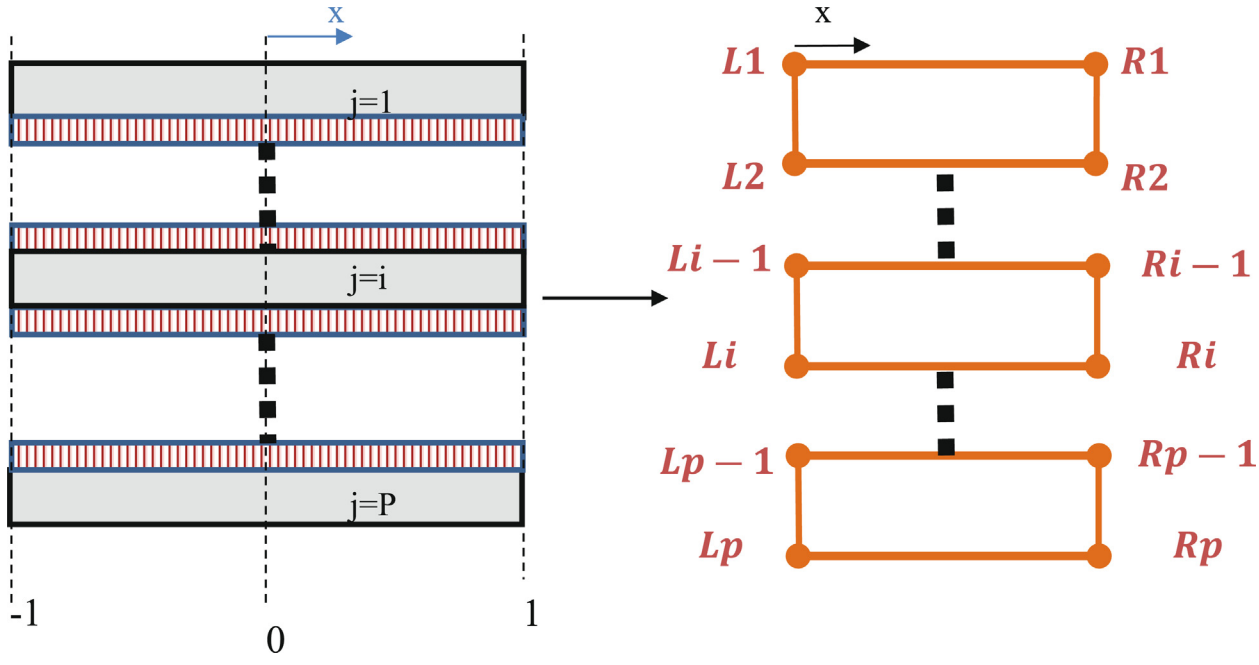

Fig. 13. ME representation of multilayered bonded joint.

$$\text{At}\xi = 1 : \begin{cases} \sum_{n=0}^{\infty} U_{1,n} = u_{R1} \\ \vdots \\ \sum_{n=0}^{\infty} U_{i,n} = u_{Ri} \\ \vdots \\ \sum_{n=0}^{\infty} U_{p,n} = u_{Rp} \end{cases} \tag{66}$$

The assembly of these three systems have been put into matrix form. Once again, the vector V_N of size $P(n_{max}+1)$ stands for the unknown coefficients vector such that:

$$\{V_N\} = \left[U_{1,0} U_{1,1} \cdots U_{1,nmax} \cdots U_{i,0} \cdots U_{i,nmax} \cdots U_{p,0} \cdots U_{p,nmax}\right]^T \tag{67}$$

Then, the matrix M_N is built by first gathering the $P(n_{max}-1)^{th}$ recursive equations, then the left P^{th} boundary conditions and finally the right P^{th} remaining equations. Finally, the matrix M_N become of the size $[P(n_{max}+1)]^2$. To finish, the vector u (of the same size as V_N) that gathers the unknown displacements of the ME is written:

$$\{u\} = \left[0 \cdots 0 u_{L1} \cdots u_{Li} \cdots u_{Lp} u_{R1} \cdots u_{Ri} \cdots u_{Rp}\right]^T \tag{68}$$

The complete system is recalled:

$$[M_N]\{V_N\} = \{u\}$$

Now, let's perform the TEPS force based approach:

In the following part, the system Eq. (63) will be written into matrix form focusing on the forces. The normal forces $Q_{L1} \cdots Q_{Lp}$ and $Q_{R1} \cdots Q_{Rp}$ are applied respectively at the left and right nodes of the ME and are unknown. First, the system Eq. (63) has been differentiated with respect to × such that:

$$\begin{cases} \frac{d^3u_1}{dx^3} + \frac{w}{A_1} ka_1 \left(\frac{du_2}{dx} - \frac{du_1}{dx}\right) = 0 \\ \vdots \\ \frac{d^3u_i}{dx^3} + \frac{w}{A_i} \left[ka_{i-1} \frac{du_{i-1}}{dx} - (ka_{i-1} + ka_i) \frac{du_i}{dx} + ka_i \frac{du_{i+1}}{dx}\right] = 0 \\ \vdots \\ \frac{d^2u_p}{dx} + \frac{w}{A_p} ka_{p-1} \left(\frac{du_{p-1}}{dx} - \frac{du_p}{dx}\right) = 0 \end{cases} \tag{69}$$

Writing this system Eq. (69) with respect to normal forces gives:

$$\begin{cases} \frac{d^2N_1}{dx^2} + wka_1 \left(\frac{N_2}{A_2} - \frac{N_1}{A_1}\right) = 0 \\ \vdots \\ \frac{d^2N_i}{dx^2} + w\left[ka_{i-1} \frac{N_{i-1}}{A_{i-1}} - (ka_{i-1} + ka_i) \frac{N_i}{A_i} + ka_i \frac{N_{i+1}}{A_{i+1}}\right] = 0 \\ \vdots \\ \frac{d^2N_p}{dx^2} + wka_{p-1} \left(\frac{N_{p-1}}{A_{p-1}} - \frac{N_p}{A_p}\right) = 0 \end{cases} \tag{70}$$

Then, like in the previous part, the system is written in terms of coefficients such that:

$$\begin{cases} \mathrm{U}_{1,n+3} + \frac{wc^2}{A_1(n+2)(n+3)} ka_1 (\mathrm{U}_{2,n+1} - \mathrm{U}_{1,n+1}) = 0 \\ \vdots \\ \mathrm{U}_{i,n+3} + \frac{wc^2}{A_i(n+2)(n+3)} [ka_{i-1}\mathrm{U}_{i-1,n+1} - (ka_{i-1} + ka_i)\mathrm{U}_{i,n+1} + ka_i \mathrm{U}_{i+1,n+1}] = 0 \\ \vdots \\ \mathrm{U}_{p,n+3} + \frac{wc^2}{A_p(n+2)(n+3)} ka_{p-1} (\mathrm{U}_{p-1,n+1} - \mathrm{U}_{p,n+1}) = 0 \end{cases} \tag{71}$$

The number of recursive equations obtained is $P(n_{max} - 2)$. As previously, in order to have a balanced number of equations, $2 \times P$ equations of force boundary conditions should be introduced.

$$\mathrm{At}\xi = -1 : \begin{cases} -\frac{A_1}{c} \sum_{n=0}^{\infty} (-1)^n (n+1) \mathrm{U}_{1,n+1} = Q_{L1} \\ \vdots \\ -\frac{A_i}{c} \sum_{n=0}^{\infty} (-1)^n (n+1) \mathrm{U}_{i,n+1} = Q_{Li} \\ \vdots \\ -\frac{A_p}{c} \sum_{n=0}^{\infty} (-1)^n (n+1) \mathrm{U}_{p,n+1} = Q_{Lp} \end{cases} \tag{72}$$

$$\text{At } \xi = 1: \begin{cases} \frac{A_1}{c} \sum_{n=0}^{\infty} (n+1) \mathrm{U}_{1,n+1} = Q_{R1} \\ \vdots \\ \frac{A_i}{c} \sum_{n=0}^{\infty} (n+1) \mathrm{U}_{i,n+1} = Q_{Ri} \\ \vdots \\ \frac{A_p}{c} \sum_{n=0}^{\infty} (n+1) \mathrm{U}_{p,n+1} = Q_{Rp} \end{cases} \tag{73}$$

Finally, the systems Eq. (71), Eq. (72) and Eq. (73) are assembled which give a system of the size Pn_{max}. Then, $2 \times P$ lines of zeros are added in order to balance the system so that its size become$P(n_{max} + 1)$. The system can now be put into matrix form. The vector V_N remains unchanged but the vector Q is defined as followed:

$$\{Q\} = \left[0 \cdots 0 Q_{L1} \cdots Q_{Li} \cdots Q_{Lp} Q_{R1} \cdots Q_{Ri} \cdots Q_{Rp}\right]^T \tag{74}$$

The complete system is thus recalled:

$$[N_N]\{V_N\} = \{Q\}$$

with the matrix N_N of the size $[P(n_{max} + 1)]^2$.

The methodology of part *2.3.2* has been applied, however, this time the vectors of the true displacement and force are now:

$$\{u\} = \left[u_{L1} \cdots u_{Li} \cdots u_{Lp} u_{R1} \cdots u_{Ri} \cdots u_{Rp}\right]^T \tag{75}$$

$$\{Q\} = \left[Q_{L1} \cdots Q_{Li} \cdots Q_{Lp} Q_{R1} \cdots Q_{Ri} \cdots Q_{Rp}\right]^T \tag{76}$$

The stiffness of any multilayered bonded joint is then the down right corner of matrix Ψ:

$$K = [N_N][M_N]^{-1} \begin{matrix} P(n_{max} - 1) \cdots P(n_{max} + 1) \\ P(n_{max} - 1) \cdots P(n_{max} + 1) \end{matrix} \tag{77}$$

3.3. Convergence and comparison

As previously, a convergence study was done and led to the choice of truncature order $n_{max} = 15$ to have fully converged results at 10^{-3} level. In this part, the validation of the multilayered bonded joint TEPS method will be done using numerical results from FE analysis.

3.3.1. Validation by finite element: Test model presentation

To validate the TEPS semi-analytical model, two models will be compared to FE analysis.

The tests correspond to an assembly of four aluminum sheets bonded together with three layers of adhesive as presented in Fig. 14 and Table 2. The left end of the adherends are clamped while the right ends remain free except for the fourth adherend where a tensile force is applied. Only the shear modulus of the glue will differ from TEST 1 to TEST 2. Indeed, it will be multiplied by 10. The FE analysis has been performed thanks to the software SAMCEF by modeling the adherends as bars and the adhesive layer as shear springs [12], which is coherent with the TEPS model that uses Volkersen assumptions (Fig. 14). The stiffnesses of springs k_u are directly related to the mesh density along the overlap [21]. For a spring element located at an abscissa × along the overlap, the stiffnesses are computed from the actual value of adhesive peel and shear modulus at the abscissa × , the adhesive thickness *ea*, the width *b* and the mesh density *L/n_BE* such as:

$$k_u(x) = m(x) \frac{L}{n\_BE} b \frac{G_a(x)}{ea} \tag{78}$$

where *m(0 < x < L) = 1* and *m(x = 0) = m(x = L) = 1/2*.

A density of *n_BE = 20* bar elements along the overlap per mm providing convergent results and the details on the approach for the FE can be found in [10].

3.3.2. TEPS scheme validation

The comparison between the FE analysis and TEPS solution will be held on the adhesive shear stress in each of the adherends, the normal forces in the adherends at the clamped region and the displacements at the free end of the adherends. The results for TEST 1 (G = 100 MPa) are firstly presented. The results of FE analysis versus TEPS method for the reaction force in the adherends at the clamped region is presented in the Table 3. The results of FE analysis versus TEPS method for the displacements of the adherends at the clamped region is presented in the Table 4. The results for the shear stresses in the three adhesives layers are depicted in the Fig. 15. This first test validates the TEPS method. Indeed, looking at Tables 3 and 4 and Fig. 15, a maximum error of 0.0003% is observed in reaction forces, of 0.0002% for displacements and 0.0005% in adhesive shear stresses.

The results for TEST 2 (G = 1000 MPa) are presented. The results of FE analysis versus TEPS method for the reaction force in the adher-

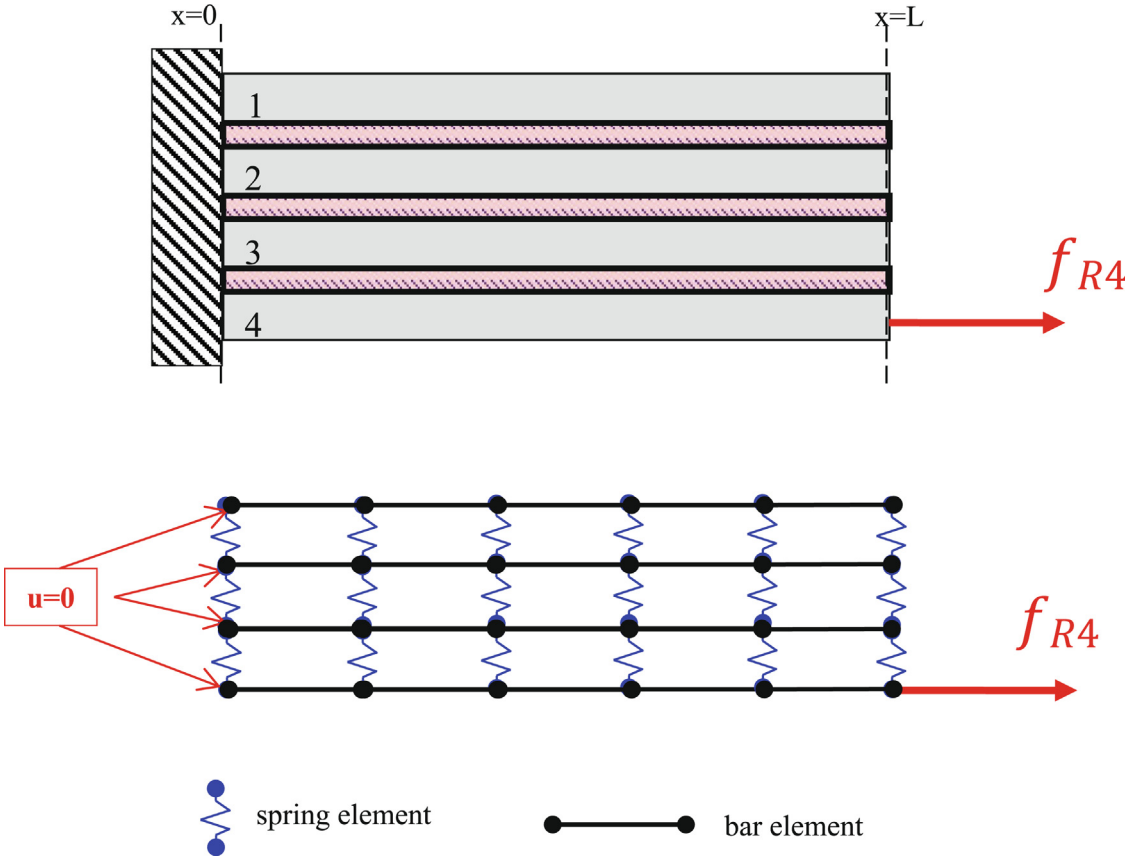

Fig. 14. Scheme of test 1 & 2 configuration.

Table 2
Mechanical and geometrical properties of test 1 & 2.

		TEST #1	TEST #2
Number of adherends	P	4	4
Length of the overlap	L	30 mm	30 mm
Width of the adherends	w	1 mm	1 mm
Thickness of the adherends	e_j	2.5 mm	2.5 mm
Young's modulus of adherends	E_j	70000 MPa	70000 MPa
Thickness of the adhesive	ea_j	0.11 mm	0.11 mm
Shear modulus of the adhesive for the first analysis	G_j	**100** MPa	**1000** MPa
Applied force (at the last layer, x = L)	f_{R4}	200 N	200 N

ends at the clamped region is presented in the Table 5. The results of FE analysis versus TEPS method for the displacements of the adherends at the clamped region is presented in Table 6. The results for the shear stresses in the three adhesives layers are depicted in the Fig. 16. This second test clearly validate the TEPS method. Indeed, looking at Tables 5 and 6 and Fig. 16, a maximum error of 0.0554% is observed in reaction forces, of 0.3822% for displacements and 0.0376% in adhesive shear stresses.

These two tests showed that the TEPS semi-analytical predictions followed exactly the predictions obtained by FE analysis. Consequently, the TEPS semi-analytical model is validated and could be used to predict multilayered metallic bonded joint behaviors. However, an accuracy of 0.0002% has no real meaning and an interesting next step could be to fix a target percentage error (which is realistic) and find the lowest truncation order *nmax* needed to reach this target. Indeed, even though TEPS method is fast, lowering its number of increment will lower the computational time.

3.3.3. ME TEPS validation

This part presents the comparison of TEPS-ME results with results from FE analysis. The configurations presented in part *3.3.2* have been used conserving the same four test cases. First, the stiffness matrix of the four-layered metallic bonded joint has been built with the methodology presented above in part 3.3.2. Then, for each of the two tests, the following Eq. (79) has been solved.

$$[K]\{u\} = \{f\}$$

Finally, at any overlap location $\times$, the shear stress in the adhesive layers and the normal forces in the adherends have been computed. These results have been compared to those obtained by FE analysis and appeared to be exactly the same as the one presented in Section 3.3.2.

Table 3
TEPS vs. FEA reaction force.

	Reaction force [N] at x = 0 (clamped end)			
Method	1st Layer	2nd Layer	3rd Layer	4th Layer
TEPS	22.6749	33.5751	57.0482	86.7018
FE analysis	22.6748	33.5751	57.0481	86.7019
Error (%)	**0.0003**	0.0000	0.0001	0.0001

Table 4
TEPS vs. FEA displacement.

	Displacements in the adherends [mm] at x = L (free end)			
Method	1st Layer	2nd Layer	3rd Layer	4th Layer
TEPS	0.0025	0.0039	0.0077	0.0202
FE analysis	0.0025	0.0039	0.0077	0.0202
Error (%)	**0.0002**	0.0001	0.0002	0.0002

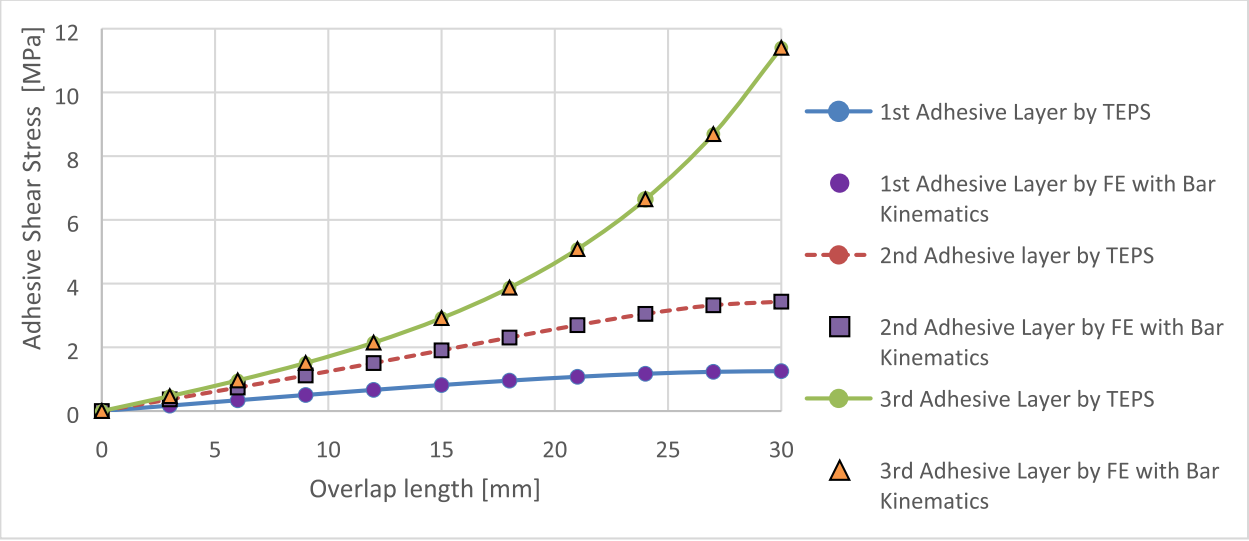

Fig. 15. Graph of adhesive shear stress obtained by FEA vs. TEPS method (TEST 1 and G = 100 MPa).

Table 5
TEPS vs. FEA reaction force.

	Reaction force [N] at x = 0 (clamped end)			
Method	1st Layer	2nd Layer	3rd Layer	4th Layer
TEPS	49.0958	49.6154	50.3720	50.9166
FE analysis	49.1000	49.6000	50.4000	50.9000
Error (%)	0.0086	0.0311	**0.0554**	0.0328

Table 6
TEPS vs. FEA displacement.

	Displacements in the adherends [mm] at x = L (free end)			
Method	1st Layer	2nd Layer	3rd Layer	4th Layer
TEPS	0.0065	0.0070	0.0083	0.0124
FE analysis	0.0065	0.0070	0.0084	0.0125
Error (%)	0.0505	0.0471	0.0400	**0.3822**

4. Application to the mechanical behavior analysis

In order to perform the behavioral analysis, the force model TEST 1 presented in numerical validation part has been used. It is composed of four aluminum sheets clamped at their left ends and glued together with an adhesive of shear modulus equal to 100 MPa. A tensile force of 200 N is applied on the fourth adherend.

4.1. Influence of adhesive thickness

To see the influence of adhesive thickness, a set of numerical tests have been applied. For each adhesive thickness, the maximum shear stress in the three adhesive layers and the normal forces in the four adherends at the clamped region have been recorded and are presented in the following Fig. 17.

The graph of the maximum shear stress Fig. 17 shows that the bigger is the adhesive thickness, the lower is the adhesive shear stress. However, the curves seem to converge which means that up to a certain value, increasing the adhesive thickness will no more decrease the maximum shear stress in the adhesive. The graph of the normal forces (Fig. 18) seems to confirm this convergence tendency. An interesting point to notice is that only the normal force in the fourth adherend increases when adhesive thickness increases. At the smallest adhesive thickness, the fourth adherend sustains only 30% of the applied load, the remaining 70% is almost evenly distributed in the three other metallic sheets. However, at the biggest adhesive thickness, the fourth adherend sustains by itself more than 80% of the applied load while the two first layers undergo only 5% of the load. This means that (up to convergence) the bigger is the adhesive thickness the less the load is transmitted to the other metallic layers.

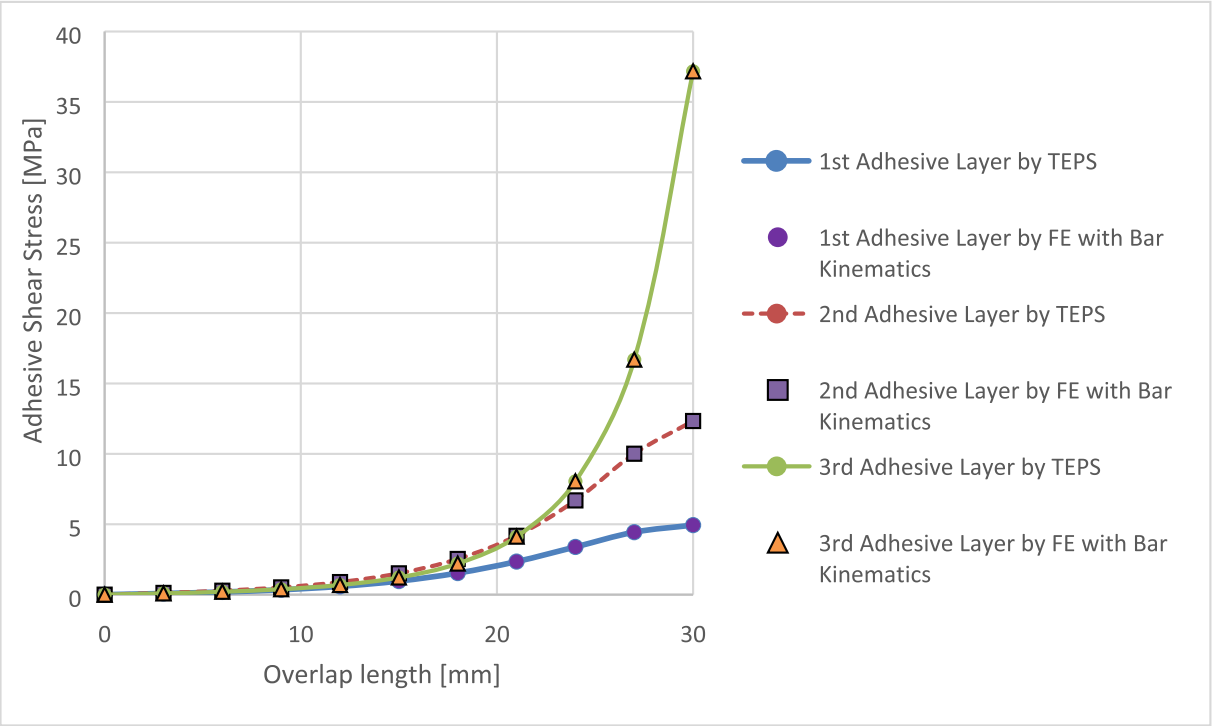

Fig. 16. Graph of adhesive shear stress obtained by FEA vs. TEPS method (TEST 2 and G = 1000 MPa).

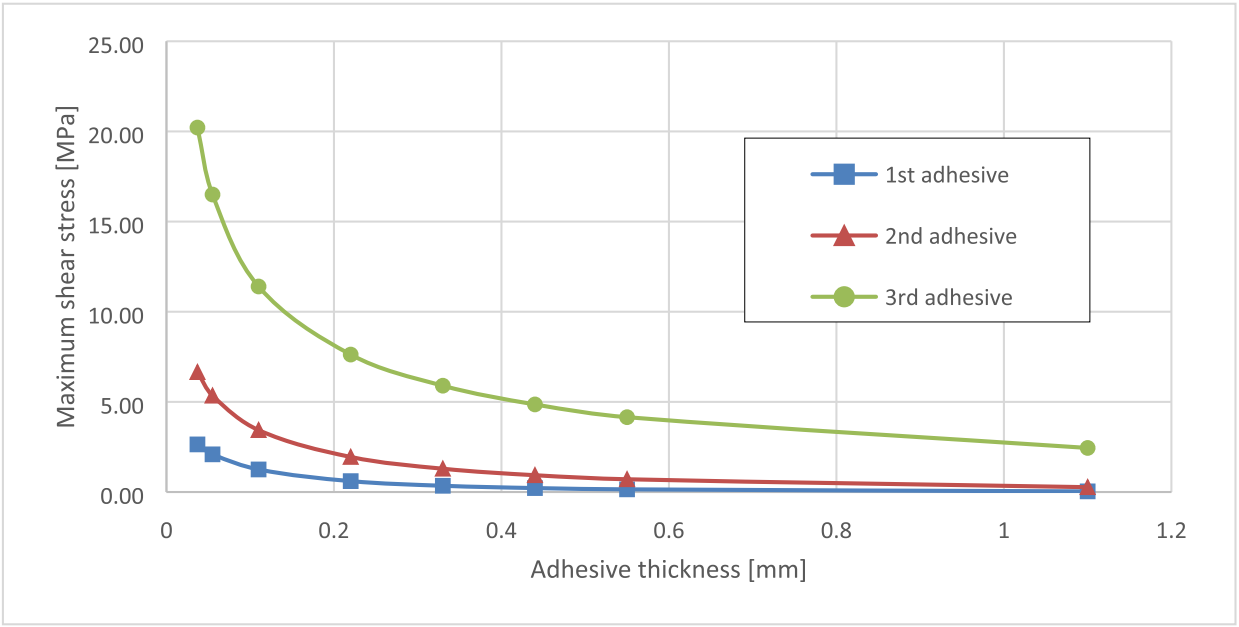

Fig. 17. Maximum shear stress vs. adhesive thickness.

4.2. Influence of overlap length

To see the influence of the overlap length, a set of numerical tests have been applied.

For each overlap length, the maximum shear stress in the three adhesive layers and the normal forces in the four adherends at the clamped region have been recorded and are presented in the following Fig. 19.

The graph of the maximum adhesive shear stress (Fig. 19) shows that increasing the overlap length will increase the adhesive shear stress. However, convergence is really fast. The normal force (Fig. 20) shows this fast convergence too. Indeed, with a small overlap length, the fourth adherend sustains almost all the tensile load (94%). Increasing the overlap balances the system so that when convergence is reached, the four adherends are evenly loaded and sustain 25% of the load each. It is important to notice that, even though at convergence the four bars sustain the same load, the adhesive shear stress is not evenly distributed through the adhesive layers.

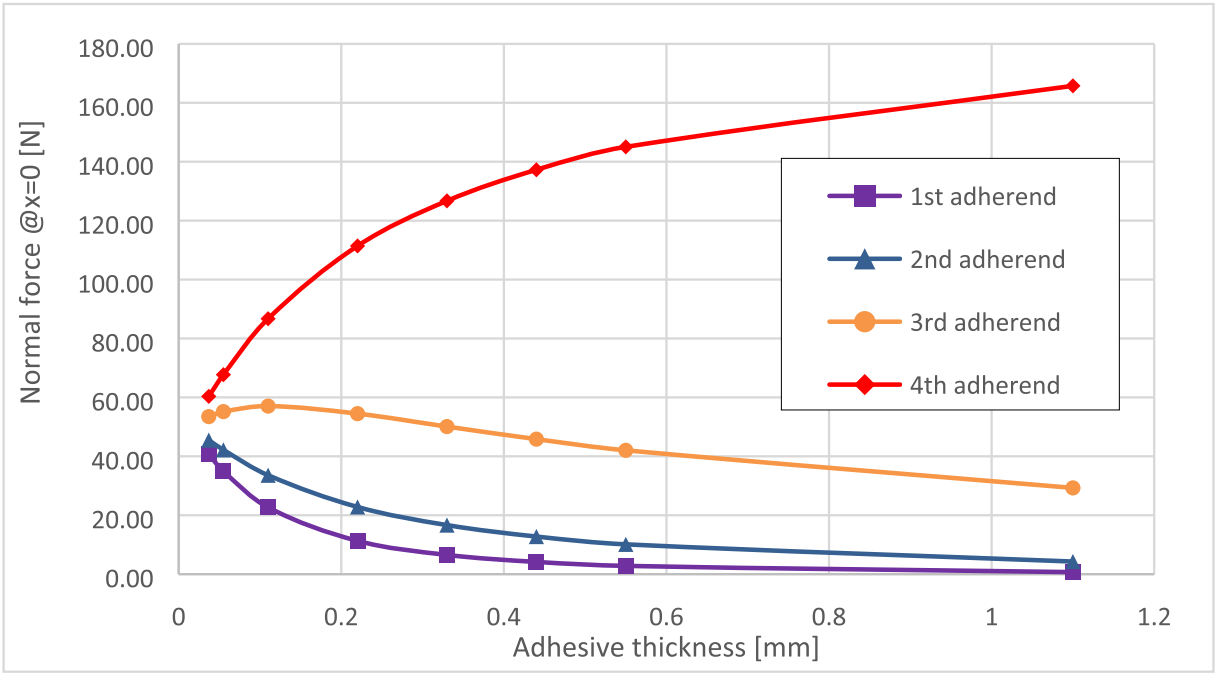

Fig. 18. Normal forces in the adherends vs. adhesive thickness.

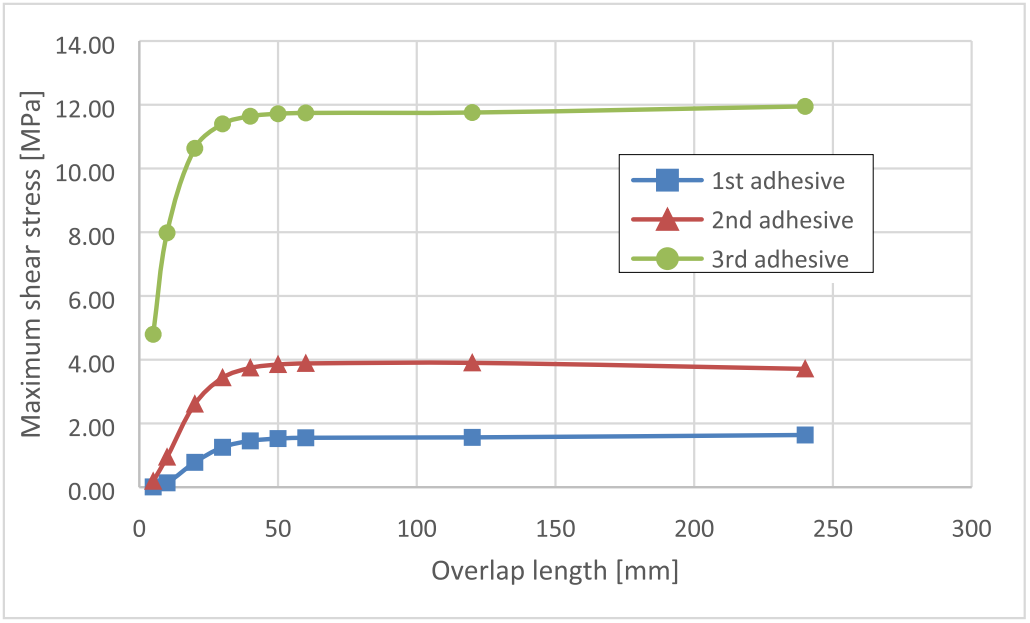

Fig. 19. Maximum shear stress vs. overlap length.

5. Conclusion

In this paper, a methodology for a simplified stress analysis of any sizes of multilayered metallic bonded joints has been presented. The assumption used are the one of Arnovljevic [17] and Volkersen's [18] classical shear lag analysis under 1D-bar kinematics (for the adherends). As an introduction, the methodology was performed for the analysis of the simplest configuration of bonded joint: the SLJ. A solution for the normal forces in the adherends and shear stress in the adhesive layer was obtained in term of a system of coupled ODEs. This system was decoupled, linearized and approximated using TEPS method. A n_{max} series truncating order was defined to choose the level of approximation. Two resolution schemes have been presented. The first one, the TEPS linear system, was easily solved semi-analytically (MATLAB code provided). A convergence study showed that convergence occurs around $n_{max} = 15$ and the results obtained were very accurate compared to the exact SLJ. The second resolution scheme was the reduction of the SLJ into ME having a stiffness matrix obtained with TEPS methods. The TEPS ME stiffness matrix was compared to the exact ME stiffness matrix and, at convergence ($n_{max} = 15$), the method was very satisfying (low errors). Then, the method used for the SLJ model was modified and parameterized to be able to analyze any sizes of multilayered metallic bonded joints. Solution have been obtained from both resolution schemes discussed previously. After performing a convergence study (giving the same results as above), results have been compared to the one of a FE analyses. The test model was a 4-layered metallic bonded joint submitted to a tensile load on one of its layers. The method gave very accurate results so that the simplified

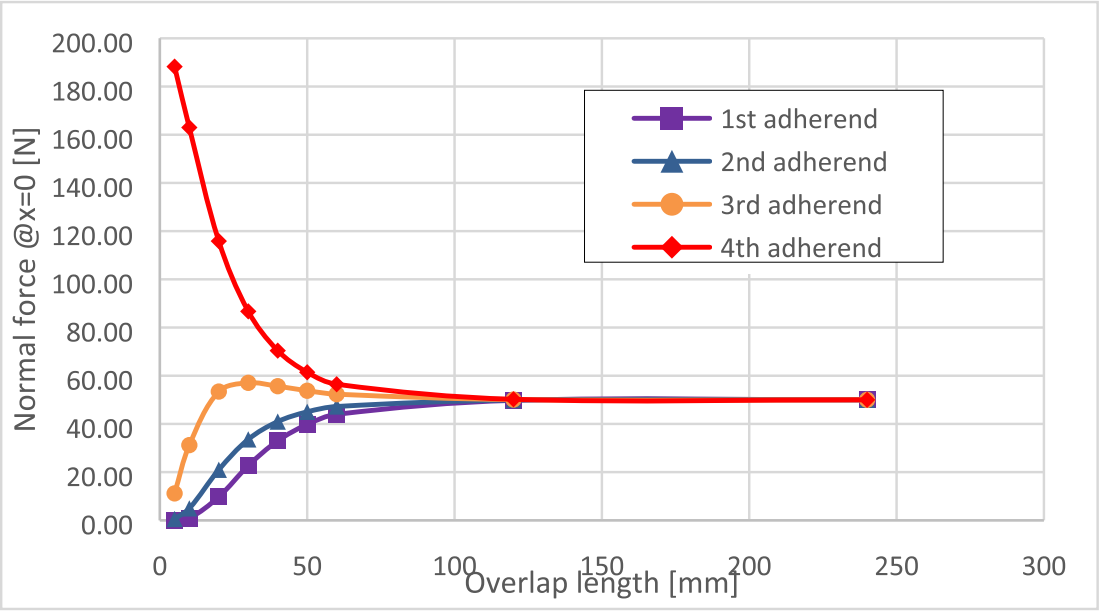

Fig. 20. Normal forces in the adherends vs. overlap length.

stress analysis tool is validated. Based on this methodology, a fully parameterized (plug-and-play) tool has been implemented for pre-sizing purpose (MATLAB code provided). In few steps, the user can build any sizes of multilayered bonded joint models, with any types of adherends and any types of adhesives (following the 1D-bar kinematics). Since a semi-analytical resolution scheme is used, the computational time and resources are extremely low compared to FE analysis (with same results). As an application, a mechanical analysis behavior was done in the paper. It has been observed that, up to a certain value, the bigger is the adhesive thickness the less the load is transmitted to the other metallic layers. Then, results tend to converge so that increasing the thickness will no more have an influence on transmission of loads between layers. Also, varying the overlap length showed that it has an influence on the load transmission across layers. Then, increasing the length will balance the normal forces in the adherends. However, the results converge quickly so that increasing the overlap length will have no effect of the load transmissibility anymore. This paper presented two fast and easy-to-use methods in order to perform simplified stress analysis on any sizes and types of multilayered metallic bonded joints for a presizing purpose. It also introduced and validated a way of building multilayered ME. These methods are interesting in the way they are methodologies having modelling flexibilities. Indeed, they could be perfectly suitable in order to build more complex models such as 1D beam kinematics one.

CRediT authorship contribution statement

Vincent Torrelli: Conceptualization, Methodology, Software, Validation, Formal analysis, Investigation, Writing - original draft. **Eric Paroissien:** Conceptualization, Methodology, Formal analysis, Investigation, Writing - original draft.

Declaration of Competing Interest

The authors declare that they have no known competing financial interests or personal relationships that could have appeared to influence the work reported in this paper.

Acknowledgement

This work has not received any specific grant.

References

[1] J.N. Reddy Mechanics of Laminated Composite Plates and Shells: Theory and Analysis 2nd ed., 2004 CRC Press. ISBN 0-8493-1592-1.
[2] Shokrieh MM, Kamali Shahri SM. Modeling residual stresses in composite materials. In: Residual stresses in composite materials. Woodhead Publishing; 2014. p. 173–93. https://doi.org/10.1533/9780857098597.1.173.
[3] Nairn J. Generalized shear-lag analysis including imperfect interfaces. Adv Compos Lett 2004. https://doi.org/10.1177/096369350401300601.
[4] Jiang G, Peters K. A shear-lag model for three-dimensional, unidirectional multilayered structures. Int J Solids Struct 2008;45(14):4049–67.
[5] Viet N, Zaki W, Umer R. Interlaminar shear stress function for adhesively bonded multi-layer metal laminates. Int J Adhes Adhes 2018;82:14–20.
[6] Pham PV, Mohareb M, Fam A. Finite element formulation for the analysis of multilayered beams based on the principle of stationary complementary strain energy. Eng Struct 2018;167:287–307.
[7] Sekmen K, Paroissien E, Lachaud F. Simplified stress analysis of multilayered adhesively bonded structures. Int J Adhes Adhes 2020;97:102497.
[8] Lélias G, Paroissien E, Lachaud F, Morlier J, Schwartz S, Gavoille C. An extended semi-analytical formulation for fast and reliable stress analysis of adhesively bonded joints. Int J Solids Struct 2015;62:18–39.
[9] Paroissien E, da Silva LFM, Lachaud F. Simplified stress analysis of functionally graded single-lap joints subjected to combined thermal and mechanical loads. Compos Struct 2018;203:85–100.
[10] Paroissien E, Lachaud F, da Silva LFM, Seddiki S. A comparison between macro-element and finite element solutions for the stress analysis of functionally graded single-lap joints. Compos Struct 2019;215:331–50.
[11] Ordonneau B, Paroissien E, Salaün M, Malrieu J, Guigue A, Schwartz S. A methodology for the computation of the macro-element stiffness matrix for the stress analysis of a lap joint with functionally graded adhesive properties. Int J Adhes Adhes 2020;97:102505.
[12] Lachaud F, Paroissien E, Michel L. Validation of a simplified analysis for the simulation of delamination of CFRP composite laminated materials under pure mode I. Compos Struct 2020;237:111897.
[13] Hart Smith, RJ, 1973. Adhesive-bonded scarf and stepped-lap joint. NASA Technical Report, CR-112237, Douglas Aircraft Company, Long Beach, CA.
[14] Carbas RJC, da Silva LFM, Madureira ML, Critchlow GW. Modelling of functionally graded adhesive joints. J Adhesion 2014;90(8):698–716.
[15] Stein N, Weißgraeber P, Becker W. Stress solution for functionally graded adhesive joints. Int J Solids Struct 2016;97–98:300–11.
[16] Stein N, Felger J, Becker W. Analytical models for functionally graded adhesive joints: a comparative study. Int J Adhes Adhes 2017;76:70–82.
[17] Arnovljevic I. Das Verteilungsgesetz der Tiefspannungen in axial beanspruchten Verbundstaben. Z.F. Archund-Ing-Wesen 1909;55:415–8.
[18] Volkersen O. Die Nietkraftverteilung in Zugbeanspruchten Nietverbindungen mit konstanten Laschenquerschnitten. Luftfahrforschung 1938;15(24):41–7.
[19] Tsai MY, Oplinger DW, Morton J. Improved theoretical solutions for adhesive lap joints. Int J Solids Struct 1998;35:1163–85.
[20] Paroissien E, Gaubert F, Da Veiga A, Lachaud F. Elasto-plastic analysis of bonded joints with macro-elements. J Adhes Sci Technol 2013;27(13):1464–98.
[21] Dechwayukul C, Rubin CA, Hahn GT. Analysis of the effects of thin sealant layers in aircraft structural joints. AIAA J 2003;41:2216–28.